J Incl Phenom Macrocycl Chem (2011) 71:593–602
DOI 10.1007/s10847-011-9996-4

ORIGINAL ARTICLE

# Controlled release of volatile (−)-menthol in nanoporous silica materials

**Jun Zhang · Meihua Yu · Pei Yuan · Gaoqing Lu · Chengzhong Yu**

Received: 29 April 2011 / Accepted: 27 May 2011 / Published online: 15 June 2011


**Abstract** In this work, a series of nanoporous silica materials have been prepared as adsorbents for volatile (−)-menthol, a molecule widely used in food, pharmacy, and cosmetics. The isothermal release properties of (−)-menthol have been investigated and correlated with the structural parameters of nanoporous absorbents. A rotary evaporation method is used to effectively load (−)-menthol into the nanopores of adsorbents and to prevent the whisker growth during the adsorption. It is demonstrated that the pore size, structure, wall thickness and surface functionality of nanoporous adsorbents are four important parameters to influence the isothermal release of (−)-menthol. By tuning these parameters of nanoporous silica adsorbents, controlled release of (−)-menthol can be achieved. A vesicular silica material with thick wall and hydrophobic functional groups is shown to possess the slowest release performance. Our contribution provides important knowledge for the future applications of nanoporous silica materials in pharmacy and cosmetics.

**Keywords** Mesoporous · Vesicle · Silica · (−)-Menthol · Isothermal release

## Introduction

Controlled release of molecules is an important topic in many applications. (−)-Menthol is an isomer of monocyclic terpene and has a long and wide history of usage in food [1, 2], pharmacy [3, 4] and cosmetic industry [5]. Due to its unique fragrance and cooling effect [6], (−)-menthol can be added to skin-contact drug formulation and cosmetics such as lotions and creams, however, the whisker growth [7] and high volatility [4] of (−)-menthol are the main obstacles for its adsorption and controlled release performance.

In the past few years, a variety of materials were used in the storage/delivery of (−)-menthol. A simple method is to prepare spray-dried powdery samples of (−)-menthol encapsulated with carbohydrates [8–10]. Soottitantawat et al. reported a microencapsulation method by spray drying, using gum arabic and modified starch as capsule materials [11]. Through this method, microcapsules with a high loading amount of (−)-menthol can be prepared, nevertheless a fraction of (−)-menthol is lost during the spray drying process with a temperature over 100 °C. Recently Sansukcharearnpon et al. reported the encapsulation of (−)-menthol with polymers [12]. The products showed a very long isothermal release period at room temperature around months. Macroporous silica aerogels were introduced for adsorption of (−)-menthol by Gorle et al. [13], where (−)-menthol exists in a crystalline state in the aerogels. It is suggested that solid adsorbent materials such as porous silica are good candidates in encapsulation applications because of their high mechanical strength, enhanced thermal stability, and negligible swelling in organic solvents.

Since the first report of M41S in 1992 [14], mesoporous siliceous materials with tunable structures, high surface areas, large pore volumes and different functionalized groups have attracted much attention for their potential applications as drug delivery devices, sorbents and catalysts [15, 16]. The wall compositions of mesoporous materials can be adjusted. For example, periodic mesoporous organosilica (PMO) materials have been prepared

J. Zhang · M. Yu · P. Yuan · G. Lu · C. Yu (✉)
ARC Centre of Excellence for Functional Nanomaterials and Australian Institute for Bioengineering and Nanotechnology, The University of Queensland, Brisbane, QLD 4072, Australia
e-mail: c.yu@uq.edu.au

containing organic groups homogeneously distributed in the silica framework [17–19]. Recently, vesicular materials with adjustable sizes, wall thickness, and shapes have been designed and prepared using a vesicular templating approach [20–25]. Both ordered mesoporous and vesicular materials have been used in drug release [16, 26]. It will be interesting to systematically compare the controlled release performance between ordered mesoporous and vesicular materials for a target molecule. Such a study, especially in the case of (−)-menthol, has not been reported to the best of our knowledge.

In the present work, six ordered mesoporous and vesicular materials were synthesized as the adsorbents of (−)-menthol. The (−)-menthol release behavior was further studied and correlated with the structures of nanoporous adsorbents. The knowledge gained from this study will be helpful for the designed synthesis of nanoporous adsorbents with advanced controlled release property.

## Experimental section

### Synthesis

Perfluorooctanoic acid (PFOA, ≥96%) was purchased from Aladdin Corp. (China). $EO_{39}BO_{47}EO_{39}$ and $EO_{34}BO_{11}EO_{34}$ [commercial name B50-6600 and B20-3800, respectively; EO is poly(ethylene oxide) and BO is poly(butylene oxide)] was received from Dow Company. P123 [$EO_{20}PO_{70}EO_{20}$, where PO is poly(propylene oxide)], cetyltrimethylammonium bromide (CTAB, 95%), tetraethyl orthosilicate (TEOS, ≥98%), 1,2-bis(trimethoxysilyl)ethane (BTME, 96%), trimethylchlorosilane (TMCS, ≥98.0%) were purchased from Sigma-Aldrich Corp. The other reagents were of analytical reagent grade.

Rod-like MCM-41 materials were synthesized according to our previous method using PFOA and CTAB as co-templates with a PFOA/CTAB weight ratio $R = 0.05$ [27]. In a typical synthesis of rod-like MCM-41 (denoted S1, see Table 1), 0.2 g of CTAB was dissolved in deionized water (96 g) with stirring at room temperature. Then 0.70 mL of aqueous NaOH solution (2 M) and 0.01 g of PFOA were added separately to the solution. The temperature of the solution was raised and kept at 80 °C before 1.34 mL of TEOS was added as the silica source. The mixture was continuously stirred for an additional 2 h. The precipitates were collected by filtration and dried at room temperature. The templates were removed by calcination at 550 °C for 5 h.

For the synthesis of rod-like SBA-15 (S2), 4.0 g of P123 was dissolved in 150 mL of HCl solution (1.6 M) to form a homogenous solution under stirring at 40 °C. To the above solution, 9.5 mL of TEOS was added under stirring. After stirring for 5 h, the resultant mixture solution was kept at static condition for 20 h and then hydrothermally treated at 100 °C for another 24 h. The final product S2 was obtained by collecting the precipitates by filtration, drying at room temperature, and calcination at 550 °C for 5 h.

A highly ordered rod-like PMO with large pores is reported by Qiao et al. using a triblock copolymer P123 as the template and BTME as an organosilica precursor in the presence of inorganic salt [28]. In the synthesis process of rod-like PMO (S3) [28], 0.5 g of P123 was dissolved in 20 g of HCl solution (0.167 M) with the addition of 1.49 g of KCl to form a homogenous solution under stirring at 38 °C. To the above solution, 0.7 g of BTME was added under stirring. After 10 min, the resultant mixture solution was kept at static condition for 24 h and then hydrothermally treated at 100 °C for another 24 h. The precipitates were filtered, washed with water, and dried in air. The templates were removed by solvent extraction in acidified ethanol (solid:liquid = 1 g:150 mL) at 60 °C for 6 h, the ratio of ethanol to HCl (36 wt%) was 150 mL:3.8 g. Extraction was repeated twice.

In the synthesis of thin wall and thick wall silica vesicles (denoted as S4 and S5, respectively) [21], 0.5 g of template (0.3 g of $EO_{34}BO_{11}EO_{34}$ plus 0.2 g of $EO_{39}BO_{47}EO_{39}$ for S4, pure $EO_{39}BO_{47}EO_{39}$ for S5) was dissolved in 30 g of pH = 4.7 NaAc–HAc buffer solution ([NaAc] = [HAc] = 0.40 M) with the addition of 0.85 g of $Na_2SO_4$

**Table 1** Physicochemical properties of silica samples

| Sample name | Morphology and annotation | $D_p$ (nm) | $V_p$ ($cm^3\ g^{-1}$) | $S_{BET}$ ($m^2\ g^{-1}$) | $\varphi$ (%) |
|---|---|---|---|---|---|
| S1 | Rods, MCM-41 | 2.4 | 0.92 | 862 | 52.3 |
| S2 | Rods, SBA-15 | 7.5 | 1.17 | 876 | 59.2 |
| S3 | Rods, PMO | 7.3 | 0.78 | 718 | 39.4 |
| S4 | Vesicle, thin wall | 11.1 | 0.88 | 427 | 40.8 |
| S5 | Vesicle, thick wall | 40.7 | 1.05 | 325 | 35.9 |
| S6 | Vesicle, thick wall, after silylation | 32.8 | 1.40 | 310 | 26.0 |

*Note* $D_p$ stands for the pore size calculated from the adsorption branch by BJH method, $V_p$ is single point adsorption total pore volume of pores and $S_{BET}$ is BET surface area, $\varphi$ is the weight loss percentage of (−)-menthol at 300 min

(0.20 M) to form a homogenous solution under stirring at 20 °C. To the above solutions, 2.08 g of TEOS was added under stirring. After stirring for 5 min, the resultant mixture solutions were kept at static conditions for 24 h and then hydrothermally treated at 100 °C for another 24 h. The precipitates were filtered, repeatedly washed with water to remove the added salts, and then dried in air. The final products were obtained by calcination at 550 °C for 5 h.

Silylated thick wall silica vesicles S6 was obtained by surface modification of S5 before calcination. The templates in as prepared S5 were removed by solvent extraction as described in the treatment of as-synthesized PMO. Approximately 1.5 g of thick wall silica vesicles after extraction was degassed in a vacuum oven ($<5 \times 10^{-4}$ Torr) at a temperature of 450 °C for 2 h. Subsequently, the samples were soaked in 5 wt% TMCS solution in toluene (solid:liquid = 1 g:50 mL) at 70 °C under stirring for 24 h. The mixture was then extensively washed with toluene and acetone to rinse away any residual chemicals. Finally, the powder was dried at 40 °C. A monolayer of TMS groups is thus covalently attached to the pore surface of siliceous vesicles [29].

### Characterization

X-ray diffraction (XRD) patterns of siliceous materials were recorded on a German Bruker D4 X-ray diffractometer with Ni-filtered Cu $K_\alpha$ radiation. The morphologies of the samples were observed using a Philip XL30 and JEOL JSM 6300F scanning electron microscope (SEM) operated at 20 and 10 kV, respectively. Transmission electron microscopy (TEM) images were obtained with a JEOL 2011 and JEOL 1010 operated at 200 and 100 kV, respectively. For TEM measurements, the samples were prepared by dispersing the powder samples in ethanol, after which they were dispersed and dried on carbon film on a Cu grid. Nitrogen adsorption/desorption isotherms were measured at 77 K by using a Micromeritics Tristar II system. The samples were degassed at 453 K overnight on a vacuum line. The Brunauer–Emmett–Teller (BET) method was utilized to calculate the specific surface areas. The pore volume and pore size distribution curves were derived from the adsorption branches of the isotherms using the Barrett–Joyner–Halanda (BJH) method. The total pore volume was calculated from the amount adsorbed at a maximum relative pressure ($P/P_0$). The Fourier transform infrared (FTIR) spectra were collected with a ThermoNicolet Nexus 6700 FTIR spectrometer.

### (−)-Menthol adsorption and isothermal release study

Crystalline (−)-menthol (99.0%) was purchased from Sigma-Aldrich Corp. A rotary evaporator was used for the adsorption of (−)-menthol into S1–S6. In a typical procedure, 0.5 g of siliceous products (S1–S6 separately in six individual batches) was added to 6.25 g of (−)-menthol–ethanol solution (8 wt%) in a long cylindrical flask, then the flask was attached to a rotary evaporator (BUCHI R-210) and evaporated at 45 °C in a vacuum system with a residual pressure of $2.25 \times 10^{-3}$ Torr until all solvent had been removed.

For comparison, (−)-menthol was recrystallized from its ethanol solution with a rotary evaporator using procedures described above without the addition of any silica. In another control experiment, similar loading procedures were carried out except that the ethanol was evaporated in an oil bath at 60 °C in open air.

An Olympus BX61 BIOL optical microscopy was used to monitor the morphology of materials before and after adsorption by different methods. Wide-angle XRD was also performed for materials before and after (−)-menthol adsorption. A Metter Toledo GC200 thermogravimetric analysis (TGA) station was used for the isothermal release study of S1–S6 after (−)-menthol adsorption at a constant temperature of 60 °C.

## Results

### Ordered mesostructured and vesicular silica materials S1–S6

Figure 1 shows the small-angle XRD patterns of ordered mesostructured S1, S2 and S3. At least three diffraction peaks can be observed in the XRD patterns of S1–S3, which can be indexed to a highly ordered 2D hexagonal mesostructure, with a cell parameter (calculated from the first XRD peak) of 4.5, 10.6, 11.2 nm, respectively. The XRD patterns of S4–S6 show no diffraction peaks (data not shown), indicating that S4–S6 do not have ordered structures. The SEM images show that S1–S3 have a rod-like morphology (Fig. 2A–C) while S4–S6 appear in aggregated particles with sizes smaller than 100 nm (Fig. 2D–F). The structure details of S1–S6 can be directly observed by TEM. Figure 3A shows the TEM image of rod-like S1 with helical and hexagonally patterned pores [27]. Figure 3B, C show rod-like S2 and S3 with the typical pattern viewed along the [110] direction of a 2D hexagonal structure, and the *d* spacing measured from TEM is in accordance with the XRD result. Figure 3D–F show the vesicular structure with diameters of ~20 nm for S4 and ~60 nm for S5, S6. The wall thickness is ~4 nm for S4 and ~15 nm for S5, S6.

Figure 4A shows the $N_2$ adsorption–desorption plots of S1–S3, the type IV isotherms are in accordance with the ordered mesostructure shown before. While a type H3 [30]

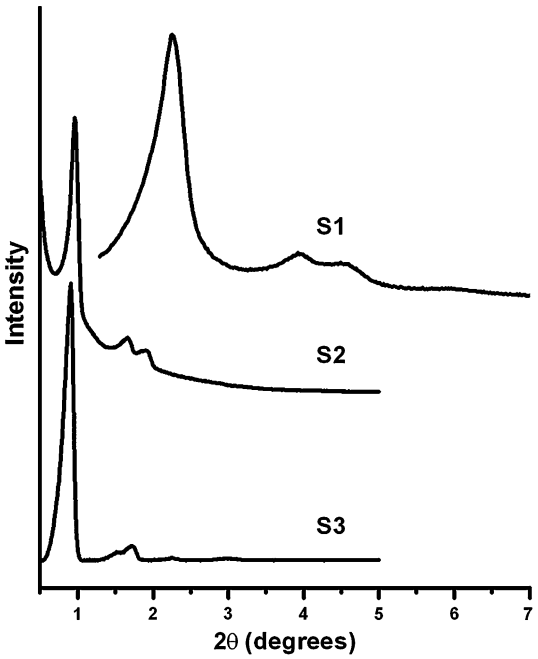


**Fig. 1** Small-angle XRD patterns of siliceous materials S1, S2 and S3

isotherm can be observed for S4–S6 with capillary condensation at high $P/P_0$, suggesting the existence of large pores. The pore size distribution (Fig. 4B) calculated from the adsorption branch by BJH method show rather narrow peaks for S1–S3 at 2.4, 7.5 and 7.3 nm, while S4–S6 have broader pore size distribution with peaks centered at 11.1, 40.7 and 32.8 nm, respectively. The pore volume, BET surface areas as well as the average pore size and morphology of S1–S6 are listed in Table 1 for comparison. Generally S1–S3 have high surface area (>700 $m^2$ $g^{-1}$) while S4–S6 have relatively low surface area (<430 $m^2$ $g^{-1}$). The above results are in accordance with previous literature reports [31].

## Silylation

Figure 5 shows the FTIR spectra of $EO_{39}BO_{47}EO_{39}$, S5 before and after extraction, and S6 after silylation. For $EO_{39}BO_{47}EO_{39}$ (Fig. 5A), the peaks at 2960 and 2870 $cm^{-1}$ can be attributed to the C–H stretching of $–CH_3$ group from block PBO [$\nu_{as}$(C–H) and $\nu_s$(C–H)] [32, 33], overlapping the C–H bond stretching of $–CH_2–$ group at

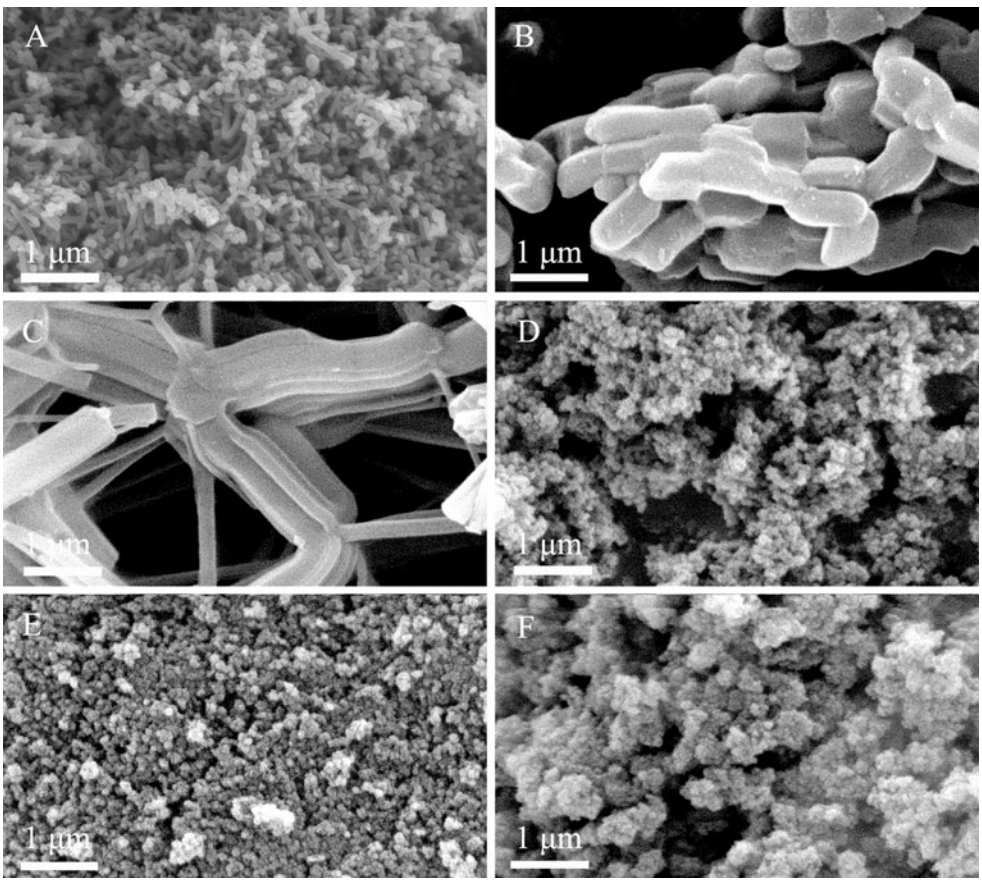


**Fig. 2** SEM images (**A**–**F**) of siliceous materials S1–S6, respectively

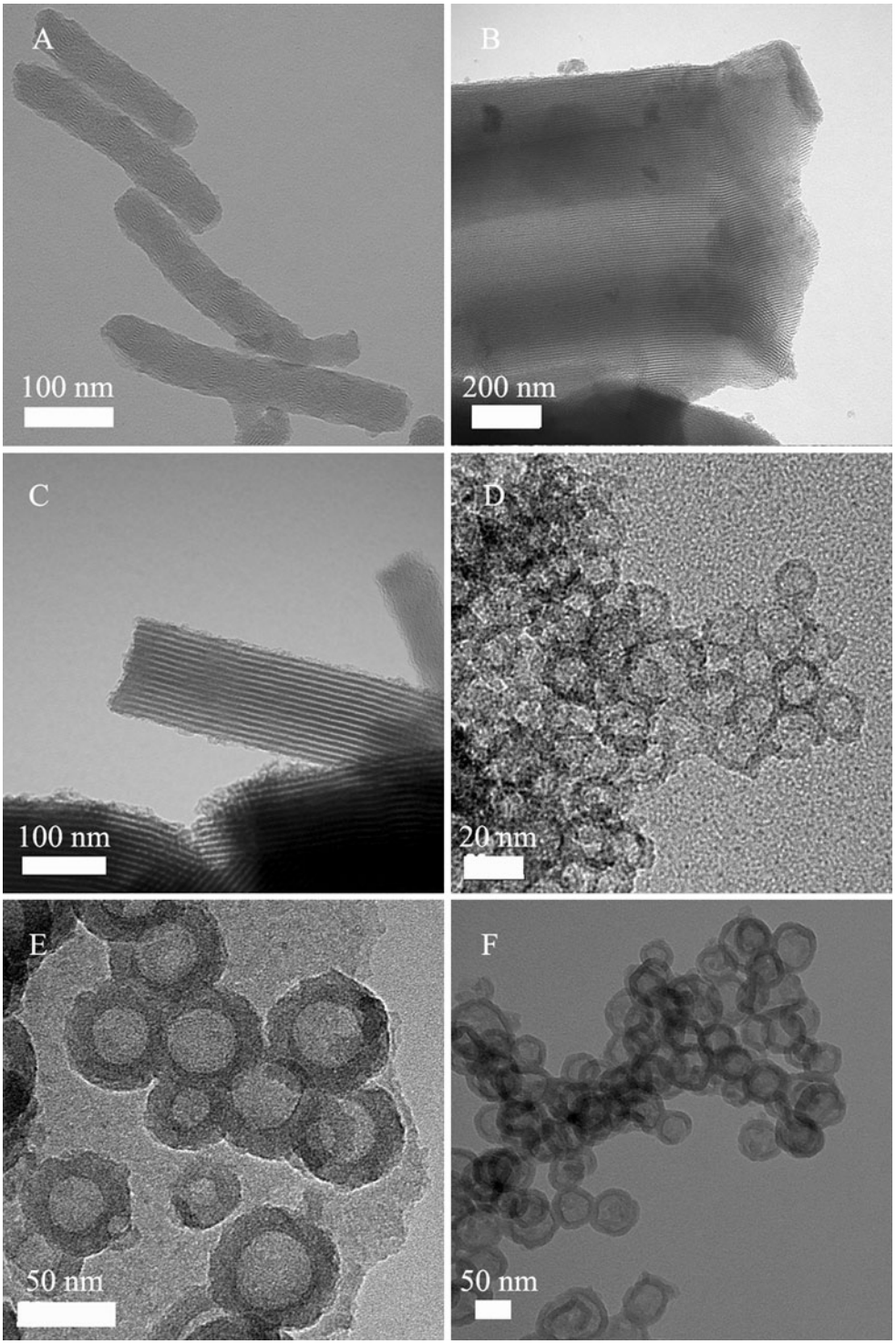


**Fig. 3** TEM images (**A–F**) of siliceous materials S1–S6, respectively

2930 and 2850 $cm^{-1}$. The peak at 1463 $cm^{-1}$ can be indexed to the scissoring band of methylene groups [$\delta(CH_2)$], and the peak at 1342 $cm^{-1}$ can be attributed to the wagging band of methylene groups [$w(CH_2)$]. The FTIR spectrum of S5 before extraction (Fig. 5B) shows the same characteristic peaks of $EO_{39}BO_{47}EO_{39}$. However, these peaks disappear after template extraction (Fig. 5C), indicating the complete removal of the template. It is noted that spectrum A also clearly shows the $–CH_2–$ twisting bands ($t_{as}(CH_2)$) at 1280, 1241 $cm^{-1}$, the C–O and C–C stretching bands ($\nu$ (C–O) and $\nu$ (C–C)) at 1099 $cm^{-1}$ and the $-CH_2–$ rocking bands ($r_{as}(CH_2)$) at 960 and 841 $cm^{-1}$.

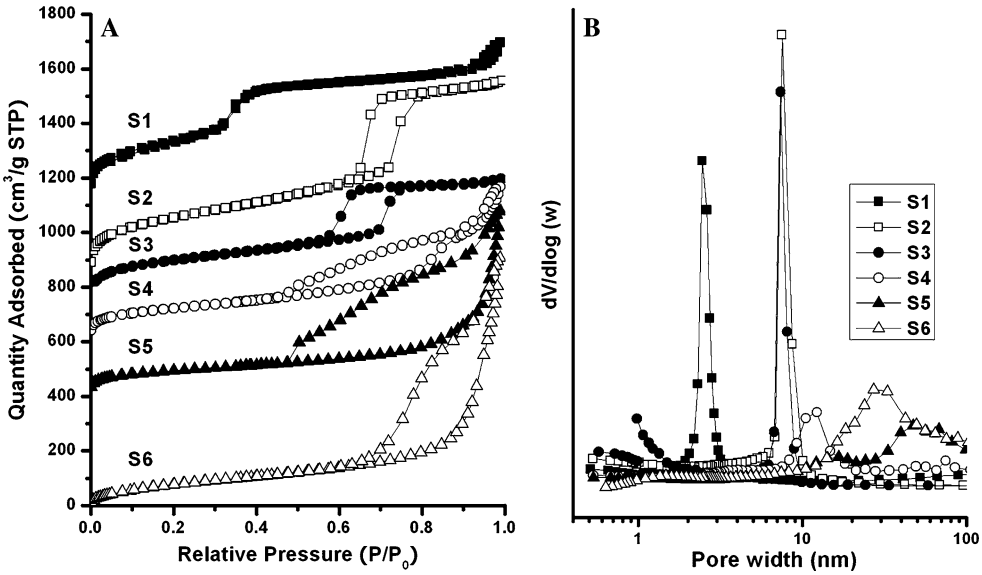


**Fig. 4** Nitrogen sorption isotherm plots (**A**) and pore size distribution curves (**B**) of siliceous materials S1–S6. The *Y*-axis value in (**A**) for S1–S5 is raised by 1100, 800, 700, 600, and 400 $cm^3\ g^{-1}$, respectively

However several peaks from the template with the wavenumber lower than 1300 $cm^{-1}$ overlap with the Si–O stretching bands of the silanol group (Fig. 5B) [34], therefore they cannot be used to confirm the template removal in Fig. 5C.

The surface silylation of S5 after extraction is based on the reaction between TMCS and surface silanol groups [14, 35]. After silylation, the FTIR spectrum of S6 (Fig. 5D) shows the absorption band at 2963 $cm^{-1}$ and a small shoulder peak at 2920 $cm^{-1}$ attributed to the attached $-(CH_3)_3$ groups [29], indicating that S6 has been successfully silylated with hydrophobic surface trimethylsilyl groups.

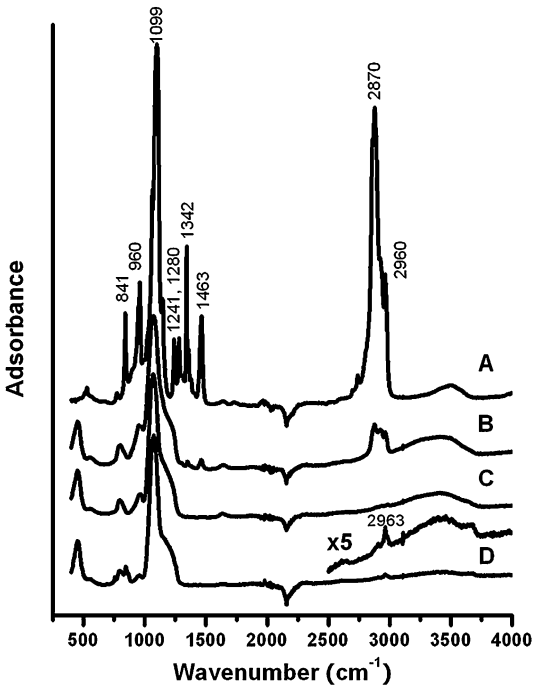


**Fig. 5** FTIR spectra of (*A*) the block copolymer $EO_{39}BO_{47}EO_{39}$ (B50-6600), (*B*, *C*) raw product of S5 before and after template extraction, (*D*) S6

## (−)-Menthol adsorption in S1–S6

The whisker growth of (−)-menthol is a common phenomenon due to its high volatility nature [4, 7]. The optical microscope images show that after rotary evaporation, (−)-menthol recrystallize into acicular whiskers in the absence of any silica nanoporous material (Fig. 6A). However, when a silica nanoporous material is used as the absorbent during the rotary evaporation process, the optical microscope images of the silica material (S6 as an example) show similar morphologies before and after adsorption (Fig. 6B, C), while no whisker can be observed after (−)-menthol adsorption and ethanol evaporation (Fig. 6C), in great contrast to that observed in Fig. 6A. It is noted that the formation of whiskers of (−)-menthol is also inhibited in the cases of S1–S5, indicating that (−)-menthol can be successfully loaded into the nanopores of S1–S6.

In a control experiment when the ethanol was evaporated in oil bath in air instead of the rotary evaporation, the optical microscopy image shows that the acicular whiskers of (−)-menthol co-exist with the silica material (Fig. 6D, also with S6 as the adsorbent). During the rotary evaporation process, it generally takes 6 h for the complete evaporation of ethanol due to the cooling reflux. This mild process ensures the complete loading of (−)-menthol into S1–S6 and prevents the formation of whiskers outside the nanopores, moreover, it prevents the loss of volatile (−)-menthol (see Fig. 8 and discussion).

The wide angle XRD technique was further used to check S6 after loading with (−)-menthol. As shown in Fig. 7A, the

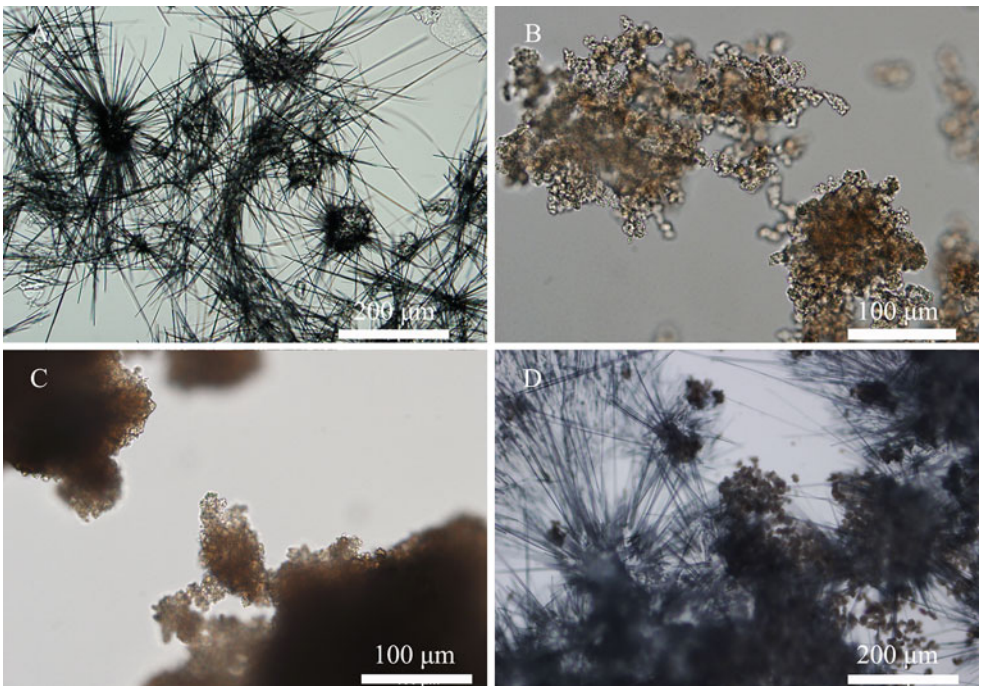


**Fig. 6** Optical microscope images for (**A**) (−)-menthol after recrystallization, (**B**, **C**) siliceous material S6 before and after (−)-menthol adsorption using a rotary evaporator, and (**D**) S6 adsorbed (−)-menthol in 60 °C oil bath for 2 h followed by solvent evaporation in air under the same condition

XRD pattern of S6/(−)-menthol shows only two broad peaks. For comparison, the XRD pattern of pure (−)-menthol is also shown in Fig. 7B. Compared to Fig. 7B, the first peak located at ∼20° in Fig. 7A is attributed to amorphous $SiO_2$ [36–38], the second peak in the range of ∼45° with low intensity is attributed to amorphous (−)-menthol dispersed in the mesopores of the silica materials. The XRD result is in accordance with the optical microscopy observation, further indicating that (−)-menthol has been successfully loaded into the silica nanoporous absorbents without whisker formation outside the adsorbents.

## Isothermal release of (−)-menthol

The isothermal release profiles of (−)-menthol from pure (−)-menthol and also S1–S6 loaded with (−)-menthol are shown in Fig. 8A, B, while the TGA profile of S4 loaded with (−)-menthol is also measured and shown in the inset of Fig. 8B. From the TGA profile of S4/(−)-menthol, the weight loss percentage of S4/(−)-menthol mixture from 20 °C to 600 °C was calculated to be 48.8%. It is noted that during the adsorption process, the weight ratio of (−)-menthol to silica adsorbent is 1:1 (0.5 g each, see Experimental Section), and there exists ∼1.0% of impurity in (−)-menthol. Therefore, the lost amount of (−)-menthol during the rotary evaporation process can be neglected and the silica/(−)-menthol feed ratio can be used to simplify the calculations of weight loss percentage in the isothermal release.

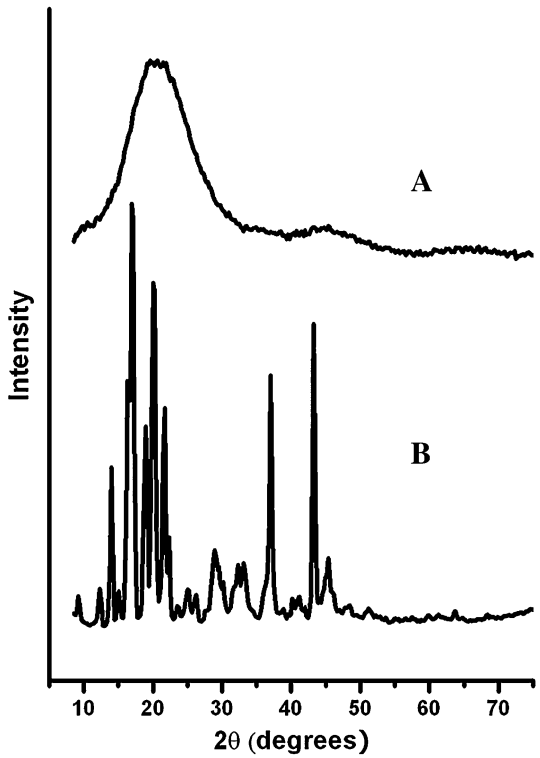


**Fig. 7** Wide-angle XRD patterns of (**A**) S6 adsorbed with (−)-menthol using a rotary evaporator and (**B**) (−)-menthol

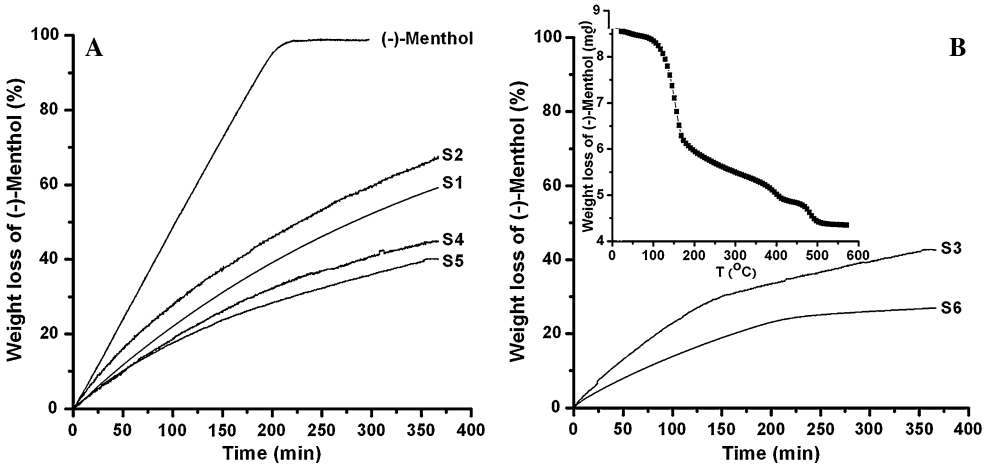


**Fig. 8** Isothermal TGA results at a constant temperature of 60 °C as a function of time of (**A**) crystalline (−)-menthol and calcined siliceous materials S1, S2, S4 and S5 loaded with (−)-menthol, (**B**) hydrophobic functionalized siliceous materials S3 and S6 loaded with (−)-menthol (*inset* is the TGA profile of S4 loaded with (−)-menthol from 20 to 600 °C)

During the isothermal release process at 60 °C, 98.6% weight percentage of (−)-menthol has been released at 200 min and there is no further weight loss after 200 min (Fig. 8A). Considering the purity of (−)-menthol used in our study is 99.0%, roughly all the (−)-menthol has been released after 200 min in a 60 °C isotherm condition.

In the cases of S1–S6 loaded with (−)-menthol, the weight loss percentage of (−)-menthol absorbed can be calculated using data shown in Fig. 8. When the isothermal release time is 300 min, the weight loss percentage of (−)-menthol adsorbed by S1, S2, S4 and S5 are 52.3, 59.2, 40.8 and 35.9%, respectively (Fig. 8A; see also Table 1). Figure 8B shows the isothermal release curves of functionalized materials S3 and S6 with a two-step release behavior. The isothermal release is faster in the first step before 134 and 207 min for S3 and S6, respectively, after that time the release rates of (−)-menthol becomes slower. The weight loss percentages of (−)-menthol adsorbed by S3 and S6 are 39.4 and 26.0% after 300 min.

## Discussion

Through this study, it is shown that all six samples (S1–S6) are good candidates in the controlled release of (−)-menthol. The pore size, structure, wall thickness and surface functionality of silica materials are important parameters to finely tune the release behaviors.

The main interaction between the (−)-menthol and the silica surface is thought to be from hydrogen bonding [13], thus the release rate of (−)-menthol is dependent on the specific surface area and the pore size of the host matrix. Large pore sizes might reduce steric diffusion resistance, so the drug release from a larger pore is more freely. The release rate of (−)-menthol is influenced by the pore size of the adsorbents [39]. It is noted that mesoporous silica S1 and S2 both have a rod-like morphology and hexagonal mesostructure, and the BET surface areas are similar ($\sim$870 $m^2$ $g^{-1}$). The difference is the pore size (2.4 and 7.5 nm, respectively). As a result, the weight percentage of (−)-menthol released at 300 min is 52.3 and 59.2%, respectively. It is concluded that a small pore size of adsorbent is favorable in the slow release of (−)-menthol, which is in agreement with previous reports [40, 41].

At a first glance, it is abnormal to note that S4 and S5 have larger pore sizes (11.1 and 40.7 nm) but slower release kinetics compared to S1 and S2 (Fig. 8A; Table 1). The four adsorbents have the same silica composition, however, S1 and S2 have open pore channels through which the adsorbed (−)-menthol can be released, while the pores of S4 and S5 are indeed cage sizes of hollow spheres that are isolated by the silica walls. It is noted that the silica walls are rich in micropores (generally <2 nm), thus the (−)-menthol can be immobilized and also released [42]. Therefore, silica adsorbents with a vesicular structure (S4 and S5) can achieve a slow release behavior compared to mesostructured silica (S1 and S2). The wall thickness of adsorbents can also influence the release rate of (−)-menthol. For the vesicular silica S4 and S5 with different wall thickness ($\sim$4 and 15 nm, respectively), the weight percentage of (−)-menthol released at 300 min is 40.8 and 35.9%, respectively. It is not surprising, because the (−)-menthol immobilized in the cages of silica vesicles has to pass the microporous silica wall during the release process. The thicker the silica wall, the longer distance (−)-menthol diffuses, leading to a slower release.

Surface functionality of silica materials is another important parameter in the controlled release of (−)-menthol. S2 and S3 both have a rod-like morphology, hexagonal mesostructure and the similar pore size (7.5 and 7.3 nm, respectively). The difference is that S3 has bridged $-C_2H_4-$ group in the siliceous matrix. Compared to pure silica S2, S3 with hydrophobic walls shows a two-step weight loss of (−)-menthol and a much lower release

percentage (59.2 and 39.4% for S2 and S3 respectively at 300 min). It is suggested that the hydrophobic interaction between the wall of S3 and (−)-menthol retards the release. To confirm this hypothesis, S6 with hydrophobic surface $-(CH_3)_3$ groups has been prepared and compared with S5 for their release performance. The isotherm release curve of S6 also shows a two-step weight loss profile, and a lower release percentage compared to S5. Attributed to its vesicular structure, microporous and thick wall, and the hydrophobic surface functionality, S6 has the slowest release rate of (−)-menthol amongst six silica nanoporous materials under study.

## Conclusions

In the present work, we systematically investigate the (−)-menthol isothermal release properties adsorbed by siliceous adsorbents with controllable structures. A rotary evaporation method has been used to load the target molecules into the adsorbents and prevent the whisker growth. We have revealed that the pore size, structure, wall thickness and surface functionality of nanoporous silica materials are four important parameters that influence the isothermal release properties of (−)-menthol. Generally small pore size, vesicular structure, thick wall and hydrophobic modification are favorable to enhance the sustainable release performance. Our concept may be applied to the controlled release of target molecules in various applications.

**Acknowledgment** We thank the Australian Research Council for support.

## References

1. Karapinar, M., Aktug, S.E.: Inhibition of foodborne pathogens by thymol, eugenol, menthol and anethole. Int. J. Food Microbiol. **4**, 161–166 (1987)
2. Yoshii, H., Sakane, A., Kawamura, D., Neoh, T.L., Kajiwara, H., Furuta, T.: Release kinetics of (−)-menthol from chewing gum. J. Incl. Phenom. Macrocycl. Chem. **57**, 591–596 (2007)
3. Gelal, A., Balkan, D., Ozzeybek, D., Kaplan, Y.C., Gurler, S., Guven, H., Benowitz, N.L.: Effect of menthol on the pharmacokinetics and pharmacodynamics of felodipine in healthy subjects. Eur. J. Clin. Pharmacol. **60**, 785–790 (2005)
4. Gelal, A., Jacob, P., Yu, L., Benowitz, N.L.: Disposition kinetics and effects of menthol. Clin. Pharmacol. Ther. **66**, 128–135 (1999)
5. Ortiz, G., Tena, M.T.: Headspace solid-phase microextraction gas chromatography-mass spectrometry method for the identification of cosmetic ingredients causing delamination of packagings. J. Chromatogr. A **1101**, 32–37 (2006)
6. Watson, H.R., Hems, R., Rowsell, D.G., Spring, D.J.: New compounds with menthol cooling effect. J. Soc. Cosmet. Chem. **29**, 185–200 (1978)
7. Yuasa, H., Ooi, M., Takashima, Y., Kanaya, Y.: Whisker growth of L-menthol in coexistence with various excipients. Int. J. Pharm. **203**, 203–210 (2000)
8. Liu, X.D., Furuta, T., Yoshii, H., Linko, P., Coumans, W.J.: Cyclodextrin encapsulation to prevent the loss of L-menthol and its retention during drying. Biosci. Biotechnol. Biochem. **64**, 1608–1613 (2000)
9. Mortenson, M.A., Reineccius, G.A.: Encapsulation and release of menthol. Part 1: The influence of OSAn modification of carriers on the encapsulation of L-menthol by spray drying. Flavour Fragr. J. **23**, 392–397 (2008)
10. Mortenson, M.A., Reineccius, G.A.: Encapsulation and release of menthol. Part 2: Direct monitoring of L-menthol release from spray-dried powders made with OSAn-substituted dextrins and gum acacia. Flavour Fragr. J. **23**, 407–415 (2008)
11. Soottitantawat, A., Takayama, K., Okamura, K., Muranaka, D., Yoshii, H., Furuta, T., Ohkawara, M., Linko, P.: Microencapsulation of L-menthol by spray drying and its release characteristics. Innov. Food Sci. Emerg. Technol. **6**, 163–170 (2005)
12. Sansukcharearnpon, A., Wanichwecharungruang, S., Leepipatpaiboon, N., Kerdcharoen, T., Arayachukeat, S.: High loading fragrance encapsulation based on a polymer-blend: preparation and release behavior. Int. J. Pharm. **391**, 267–273 (2010)
13. Gorle, B.S.K., Smirnova, I., Mchugh, M.A.: Adsorption and thermal release of highly volatile compounds in silica aerogels. J. Supercrit. Fluids. **48**, 85–92 (2009)
14. Kresge, C.T., Leonowicz, M.E., Roth, W.J., Vartuli, J.C., Beck, J.S.: Ordered mesoporous molecular-sieves synthesized by a liquid-crystal template mechanism. Nature **359**, 710–712 (1992)
15. Tao, Y.S., Kanoh, H., Abrams, L., Kaneko, K.: Mesopore-modified zeolites: preparation, characterization, and applications. Chem. Rev. **106**, 896–910 (2006)
16. Wang, S.B.: Ordered mesoporous materials for drug delivery. Microporous Mesoporous Mater. **117**, 1–9 (2009)
17. Asefa, T., Maclachlan, M.J., Coombs, N., Ozin, G.A.: Periodic mesoporous organosilicas with organic groups inside the channel walls. Nature **402**, 867–871 (1999)
18. Inagaki, S., Guan, S., Fukushima, Y., Ohsuna, T., Terasaki, O.: Novel mesoporous materials with a uniform distribution of organic groups and inorganic oxide in their frameworks. J. Am. Chem. Soc. **121**, 9611–9614 (1999)
19. Melde, B.J., Holland, B.T., Blanford, C.F., Stein, A.: Mesoporous sieves with unified hybrid inorganic/organic frameworks. Chem. Mater. **11**, 3302–3308 (1999)
20. Hubert, D.H.W., Jung, M., German, A.L.: Vesicle templating. Adv. Mater. **12**, 1291–1294 (2000)
21. Yu, M.H., Zhang, J., Yuan, P., Wang, H.N., Liu, N., Wang, Y.H., Yu, C.Z.: Preparation of siliceous vesicles with adjustable sizes, wall thickness, and shapes. Chem. Lett. **38**, 442–443 (2009)
22. Wang, H.N., Wang, Y.H., Zhou, X., Zhou, L., Tang, J., Lei, J., Yu, C.: Siliceous unilamellar vesicles and foams by using block-copolymer cooperative vesicle templating. Adv. Funct. Mater. **17**, 613–617 (2007)
23. Zhang, Y., Yu, M.H., Zhu, L., Zhou, X.F., Zhao, Q.F., Li, H.X., Yu, C.Z.: Organosilica multilamellar vesicles with tunable number of layers and sponge-like walls via one surfactant templating. Chem. Mater. **20**, 6238–6243 (2008)
24. Yu, M.H., Wang, H.N., Zhou, X.F., Yuan, P., Yu, C.Z.: One template synthesis of raspberry-like hierarchical siliceous hollow spheres. J. Am. Chem. Soc. **129**, 14576–14577 (2007)
25. Yu, M.H., Yuan, P., Zhang, J., Wang, H.N., Zhang, Y., Hu, Y.F., Wang, Y.H., Yu, C.Z.: A bioinspired route to various siliceous vesicular structures. J. Nanosci. Nanotechnol. **10**, 612–615 (2010)
26. Liu, J., Hartono, S.B., Jin, Y.G., Li, Z., Lu, G.Q., Qiao, S.Z.: A facile vesicle template route to multi-shelled mesoporous silica hollow nanospheres. J. Mater. Chem. **20**, 4595–4601 (2010)

27. Yang, S., Zhao, L.Z., Yu, C.Z., Zhou, X.F., Tang, J.W., Yuan, P., Chen, D.Y., Zhao, D.Y.: On the origin of helical mesostructures. J. Am. Chem. Soc. **128**, 10460–10466 (2006)
28. Qiao, S.Z., Yu, C.Z., Xing, W., Hu, Q.H., Djojoputro, H., Lu, G.Q.: Synthesis and bio-adsorptive properties of large-pore periodic mesoporous organosilica rods. Chem. Mater. **17**, 6172–6176 (2005)
29. Zhao, X.S., Lu, G.Q.: Modification of MCM-41 by surface silylation with trimethylchlorosilane and adsorption study. J. Phys. Chem. B **102**, 1556–1561 (1998)
30. Seaton, N.A.: Determination of the connectivity of porous solids from nitrogen sorption measurements. Chem. Eng. Sci. **46**, 1895–1909 (1991)
31. Zhang, J., Yu, M.H., Yuan, P., Wang, H.N., Qian, K., Tan, L., Wang, Y.H., Yu, C.Z.: Tuning cooperative vesicle templating and liquid crystal templating simply by varying silica source. J. Mater. Res. **25**, 648–657 (2010)
32. Su, Y.L., Wang, J., Liu, H.Z.: FTIR spectroscopic investigation of effects of temperature and concentration on PEO–PPO–PEO block copolymer properties in aqueous solutions. Macromolecules **35**, 6426–6431 (2002)
33. Dissanayake, M., Frech, R.: Infrared spectroscopic study of the phases and phase-transitions in poly(ethylene oxide) and poly(ethylene oxide)-lithium trifluoromethanesulfonate complexes. Macromolecules **28**, 5312–5319 (1995)
34. Muroya, M.: Correlation between the formation of silica skeleton structure and Fourier transform reflection infrared absorption spectroscopy spectra. Colloids Surf. A **157**, 147–155 (1999)
35. Beck, J.S., Vartuli, J.C., Roth, W.J., Leonowicz, M.E., Kresge, C.T., Schmitt, K.D., Chu, C.T.W., Olson, D.H., Sheppard, E.W., Mccullen, S.B., Higgins, J.B., Schlenker, J.L.: A new family of mesoporous molecular-sieves prepared with liquid-crystal templates. J. Am. Chem. Soc. **114**, 10834–10843 (1992)
36. Yang, J., Zhou, L.A., Zhao, L.Z., Zhang, H.W., Yin, J.N., Wei, G.F., Qian, K., Wang, Y.H., Yu, C.Z.: A designed nanoporous material for phosphate removal with high efficiency. J. Mater. Chem. **21**, 2489–2494 (2011)
37. Yang, C.M., Liu, P.H., Ho, Y.F., Chiu, C.Y., Chao, K.J.: Highly dispersed metal nanoparticles in functionalized SBA-15. Chem. Mater. **15**, 275–280 (2003)
38. Sauer, J., Marlow, F., Spliethoff, B., Schuth, F.: Rare earth oxide coating of the walls of SBA-15. Chem. Mater. **14**, 217–224 (2002)
39. Andersson, J., Rosenholm, J., Areva, S., Linden, M.: Influences of material characteristics on ibuprofen drug loading and release profiles from ordered micro- and mesoporous silica matrices. Chem. Mater. **16**, 4160–4167 (2004)
40. Horcajada, P., Ramila, A., Perez-Pariente, J., Vallet-Regi, M.: Influence of pore size of MCM-41 matrices on drug delivery rate. Microporous Mesoporous Mater. **68**, 105–109 (2004)
41. Qu, F.Y., Zhu, G.S., Huang, S.Y., Li, S.G., Sun, J.Y., Zhang, D.L., Qiu, S.L.: Controlled release of captopril by regulating the pore size and morphology of ordered mesoporous silica. Microporous Mesoporous Mater. **92**, 1–9 (2006)
42. Zhu, J., Tang, J.W., Zhao, L.Z., Zhou, X.F., Wang, Y.H., Yu, C.Z.: Ultrasmall, well-dispersed, hollow siliceous spheres with enhanced endocytosis properties. Small **6**, 276–282 (2010)